

Myeong-Jin Kim, MD²
Donald G. Mitchell, MD
Katsuyoshi Ito, MD³
Eric K. Outwater, MD

Index terms:

Bile ducts, abnormalities, 76.28
Bile ducts, calculi, 76.28
Bile ducts, diseases, 76.28
Bile ducts, stenosis or obstruction, 76.28
Gastrointestinal tract, neoplasms, 70.30
Magnetic resonance (MR), comparative studies, 76.121412, 76.121415, 76.12149
Receiver operating characteristic (ROC) curve

Radiology 2000; 214:173–181

Abbreviations:

A_z = area under the receiver operating characteristic curve
ERCP = endoscopic retrograde cholangiopancreatography
GRE = gradient-recalled echo
MRCP = MR cholangiopancreatography
ROC = receiver operating characteristic
SE = spin echo

¹ From the Department of Radiology, Thomas Jefferson University Hospital, Rm 1096, Main Bldg, 132 S 10th St, Philadelphia, PA 19107-5244. Received February 24, 1999; revision requested April 23; revision received May 14; accepted August 23. **Address reprint requests to** D.G.M. (e-mail: donald.mitchell@mail.tju.edu).

² Current address: Department of Diagnostic Radiology, Research Institute of Radiological Science, Yonsei University College of Medicine, Seoul, Korea.

³ Current address: Department of Radiology, Yamaguchi University School of Medicine, Yamaguchi, Japan.

© RSNA, 2000

Author contributions:

Guarantor of integrity of entire study, M.J.K.; study concepts, M.J.K., D.G.M., E.K.O.; study design, M.J.K., D.G.M.; definition of intellectual content, M.J.K., D.G.M., E.K.O.; literature research, M.J.K.; clinical studies, M.J.K., K.I.; data acquisition and analysis, M.J.K.; statistical analysis, M.J.K.; manuscript preparation, M.J.K.; manuscript editing and review, M.J.K., D.G.M., E.K.O.

Biliary Dilatation: Differentiation of Benign from Malignant Causes—Value of Adding Conventional MR Imaging to MR Cholangiopancreatography¹

PURPOSE: To determine the value of conventional T1- and T2-weighted images and gadolinium-enhanced dynamic magnetic resonance (MR) images as a supplement to MR cholangiopancreatographic (MRCP) images in differentiation of benign from malignant causes of biliary dilatation.

MATERIALS AND METHODS: MR studies in 62 patients with biliary dilatation with proved causes included conventional T1- and less heavily T2-weighted images, as well as gadolinium-enhanced dynamic images and heavily T2-weighted MRCP images. Two radiologists reviewed MRCP images alone, MRCP images with nonenhanced T1- and T2-weighted MR images, and MRCP images with nonenhanced and gadolinium-enhanced dynamic images.

RESULTS: For differentiation of benign from malignant causes of biliary dilatation, the area under the receiver operating characteristic curve (A_z) was significantly ($P < .05$) larger for MRCP images interpreted with T1- and T2-weighted images (0.9547 for reader 1, 0.8404 for reader 2) than for MRCP images alone (0.8144 for reader 1, 0.8122 for reader 2). The addition of gadolinium-enhanced dynamic MR images to MRCP images with nonenhanced T1- and T2-weighted images did not significantly increase accuracy ($A_z = 0.9554$ for reader 1 and 0.8650 for reader 2), but the level of confidence was increased in 17%–24% of cases.

CONCLUSION: Use of nonenhanced T1- and less heavily T2-weighted images with MRCP images significantly improved the diagnostic accuracy of MR examinations of pancreaticobiliary disease.

Magnetic resonance (MR) cholangiopancreatography (MRCP) has become an important diagnostic procedure in evaluation of pancreaticobiliary ductal abnormalities (1). The sensitivity of MRCP in the detection of choledocholithiasis has been reported as 90%–100%, comparable to that of endoscopic retrograde cholangiopancreatography (ERCP) (2–7). Assessment of the presence and level of obstruction also have been reported as highly accurate (8–14). However, the reported accuracy in differentiation of benign from malignant obstruction has varied 30%–98% (1,8–15).

The combination of imaging sequences might have influenced the diagnostic capability of MR examination: Some authors (1,8,10,13) evaluated the diagnostic ability of MRCP images in conjunction with conventional T1- and less heavily T2-weighted images, whereas others (2,9,11,12) evaluated the MRCP images alone. Conventional T1- and T2-weighted images allow evaluation of extraductal soft tissue, which may increase the diagnostic accuracy by demonstrating extension of tumor, lymphadenopathy, or metastasis in addition to depiction of tumor itself (16). However, use of conventional T1- and T2-weighted images in addition to cholangiographic images increases imaging time

and cost and decreases patient throughput. To our knowledge, no studies have specifically addressed the added value of using conventional MR images with MRCP images. The purpose of this study was to determine the added value of conventional T1- and T2-weighted images and gadolinium-enhanced dynamic MR images compared with MRCP images alone in differentiation of benign from malignant causes of biliary dilatation.

MATERIALS AND METHODS

Reports from our radiology information database from March 1997 to November 1998 were reviewed to identify patients who underwent abdominal MR imaging with MRCP and showed dilatation of the extrahepatic bile duct at MR imaging. Examination results in 62 patients who had a histopathologically or clinically confirmed cause of biliary dilatation were retrieved. The reasons for MR imaging were as follows: evaluation of bile ducts with or without pancreatic ductal dilatation detected at ultrasonography (US) in 20 cases, evaluation of pancreatic mass detected or suspected at computed tomography (CT) or US in 18 cases, differentiation of bile duct mass and calculi in two cases, clarification of undetermined abnormalities at ERCP in five cases, and other clinical reasons for which pancreaticobiliary disease was suspected on the basis of symptoms and history in 17 cases in which imaging data obtained before MR imaging at another institution were not available. Dilatation of the biliary tree was defined as larger than 7 mm in maximal diameter in patients without history of cholecystectomy who were younger than 60 years, 9 mm in patients without prior cholecystectomy who were 60 years or older, and 10 mm in patients with prior cholecystectomy.

There were 20 male patients and 42 female patients (age range, 14–87 years; mean age, 63 years). Twenty-seven patients had malignant lesions: pancreatic carcinoma ($n = 21$), ampullary carcinoma ($n = 3$), bile duct carcinoma ($n = 2$), or duodenal carcinoma ($n = 1$). Thirty-five patients had benign lesions: nonspecific biliary dilatation ($n = 24$); annular pancreas ($n = 1$); Caroli disease ($n = 1$); ampullary stricture or inflammation ($n = 5$), with ($n = 2$) or without ($n = 3$) chronic pancreatitis; or choledocholithiasis ($n = 4$). All bile duct or ampullary carcinomas and the duodenal carcinoma were confirmed by means of surgery.

Among 21 pancreatic carcinomas, 19

cases were confirmed by means of surgery or biopsy, and two were diagnosed by means of other imaging modalities and expected clinical course. Among the benign lesions, one case of pancreatitis with fibrosis was confirmed by means of surgery, and four cases of inflammatory ampullary stricture were diagnosed by means of biopsy and follow-up examinations for more than 6 months that disclosed no evidence of malignancy. Choledocholithiasis was confirmed by means of ERCP with biopsy in indicated cases. The one case of annular pancreas and the one case of Caroli disease were diagnosed by means of characteristic imaging findings and clinical setting.

Nonspecific biliary dilatation was defined as biliary dilatation without evidence of obstructive disease, and more than 6 months of follow-up clinical and imaging findings without evidence of malignancy. Among the 24 cases of nonspecific biliary dilatation, malignancy was excluded at surgery for other reasons—two at resection of distal pancreatic cystic neoplasm and one at cholecystectomy. The remaining 21 cases of nonspecific biliary dilatation were diagnosed by means of imaging findings, including ERCP, CT, and absence of change at follow-up examinations. Cholecystectomy was performed previously in two of these patients. In one case, history of Crohn disease was present, and primary sclerosing cholangitis with ampullary stenosis was suggested clinically.

TABLE 1
Interobserver Variability in Confidence Ratings

Images	κ Value
MRCP only	0.7144
MRCP with T1- and T2-weighted	0.6370
MRCP, T1- and T2-weighted, and dynamic	0.6234

TABLE 2
Reader A_z Values for Differentiation of Benign from Malignant Lesions

Reader	MRCP Images Only	MRCP Images with T1- and T2-weighted Images	MRCP Images, T1- and T2-weighted Images, and Dynamic Images
1	0.8243 \pm 0.0544	0.9560 \pm 0.0281	0.9554 \pm 0.0262
2	0.8122 \pm 0.0561	0.8897 \pm 0.0468	0.8650 \pm 0.0778

Note.—Data are A_z values \pm SD.

MR Imaging

All MR imaging was performed with a 1.5-T superconducting system (Signa; GE Medical Systems, Milwaukee, Wis) by using a phased-array torso coil.

MRCP examinations in which heavily T2-weighted sequences were used were performed with the two-dimensional fast spin-echo (SE) sequence in 34 cases and with a single-shot fast SE sequence in 28 cases. MRCP images were obtained in the coronal plane in 28 cases, in the transverse plane in seven cases, and in both planes in 27 cases. Fast SE MRCP examinations were performed with the following parameters: 12,000–15,000/252–260 (repetition time msec/echo time msec [effective]), 3-mm section thickness with no gap, and 256 \times 256 matrix. Single-shot fast SE MRCP examinations were performed with the following parameters: ∞ /392–640, 4–5-mm section thickness with no gap, and 256 \times 160–192 matrix. Field of view was adjusted to the patient's body habitus: 280–340 mm for transverse images and 260–380 mm for coronal images. The time of acquisition was 5 minutes 36 seconds to 8 minutes for fast SE MRCP and 25–30 seconds for single-shot fast SE MRCP. The image data were then transferred to a workstation (GE Medical

TABLE 3
Statistical Significance of the Difference in Interpretation among Image Sets for Each Reader

Images	Reader 1	Reader 2
MRCP only versus MRCP with T1- and T2-weighted	.0025	.0419
MRCP with T1- and T2-weighted versus MRCP, T1- and T2-weighted, and dynamic	.7713	.2247

Note.—Data are P values.

Systems) for three-dimensional cholangiographic image reconstruction with a maximum intensity projection algorithm. All images were reviewed with teleradiologic software (RATIONAL IMAGING version 4.0; Intuitive Software Technology, West Hills, Calif) installed on Unix operating systems (Sun Microsystems, Palo Alto, Calif).

Standard nonenhanced T2-weighted imaging was performed with the fast SE sequence in 27 cases, with single-shot fast SE in 11 cases, and with both in 24 cases. For less heavily T2-weighted fast SE images, the following parameters were used: 5,000–12,000/96–144, 7–8-mm section thickness, 1–2-mm gap, and 256×256 matrix. For T2-weighted images in which the single-shot fast SE sequence was used, the following parameters were used: $\infty/93.4$ –188.9, 6–9-mm section thickness, 0–2 mm gap, and 256×128 –192 matrix. Field of view for these images was the same as that used for MRCP images.

Nonenhanced T1-weighted imaging

was performed with in-phase ($n = 60$) or opposed-phase ($n = 39$) spoiled gradient-recalled echo (GRE) techniques, a three-dimensional GRE technique with fat saturation ($n = 22$), and/or SE techniques ($n = 3$). All T1-weighted images were acquired in the transverse plane. The field of view was identical to that of the T2-weighted transverse images. When GRE techniques were used for T1-weighted images, parameters were chosen individually in an effort to optimize each for a 20–25-second suspended breath hold. Two-dimensional GRE opposed-phase sequences were performed during a single suspended breath hold, whereas in-phase two-dimensional GRE sequences required two suspended breath holds. Twenty to 30 sections were obtained to cover the entire liver and pancreas with a section thickness of 6–9 mm and a 0–1.5-mm intersection gap for the in-phase and opposed-phase two-dimensional GRE sequences. Other imaging parameters for the two two-dimen-

sional sequences were as follows: 110–150/1.5–1.8 for opposed-phase images, 110–150/4.2 for in-phase images, a flip angle of 90° , 256×160 matrix, a receive bandwidth of plus or minus 32 kHz, and one signal acquired.

Three-dimensional GRE images were obtained with a gadolinium-enhanced three-dimensional fast GRE sequence with use of a fat-selective inversion pulse. Imaging parameters were as follows: 6.9–7.7/2.2–3.2/26–31 (inversion time msec), and a flip angle of 15° – 20° . The number of partitions was 30–44, with a partition thickness of 5–7 mm. In most cases, the “section zip” option, or zero filling of k space in the section-encoding axis, was used to attain half-thickness overlapping of sections; therefore, images were reconstructed with a 2.5–3.0-mm interval in those cases. The upper two and lower two images were disregarded automatically during the reconstruction; therefore, a total of 52–80 images was obtained. The matrix was 256×128 or 256×160 . In three cases in which a T1-weighted SE sequence was used, imaging parameters were as follows: 466.7–500/9–11, 8–9-mm section thickness, 1–2-mm gap, and 256×160 –192 matrix.

Gadolinium-enhanced dynamic imaging was performed with use of 0.1 mmol of gadopentetate dimeglumine (Magnevist; Berlex Laboratories, Wayne, NJ) per kilogram of body weight in a two-dimensional GRE opposed-phase sequence in 34 cases and in a three-dimensional GRE sequence in 21 cases. Arterial, venous, and delayed-phase images were serially obtained 20–30 seconds after the injection of contrast material. The total imaging time was approximately 60 minutes.

Imaging Analysis

Images were reviewed on a teleradiologic workstation monitor. Two readers (M.J.K., K.I.) with more than 3 years of experience with MRCP examinations independently reviewed the images in three steps. Neither reader was involved in the prospective clinical interpretation of the studies. All cases were reviewed randomly without providing clinical data or final diagnosis.

The readers first reviewed the coronal and/or transverse MRCP images with maximum intensity projection images and used a five-point scale to assign a confidence level to their evaluation of the cause of the biliary abnormality: 1, definitely benign; 2, probably benign; 3, possibly malignant; 4, probably malignant;

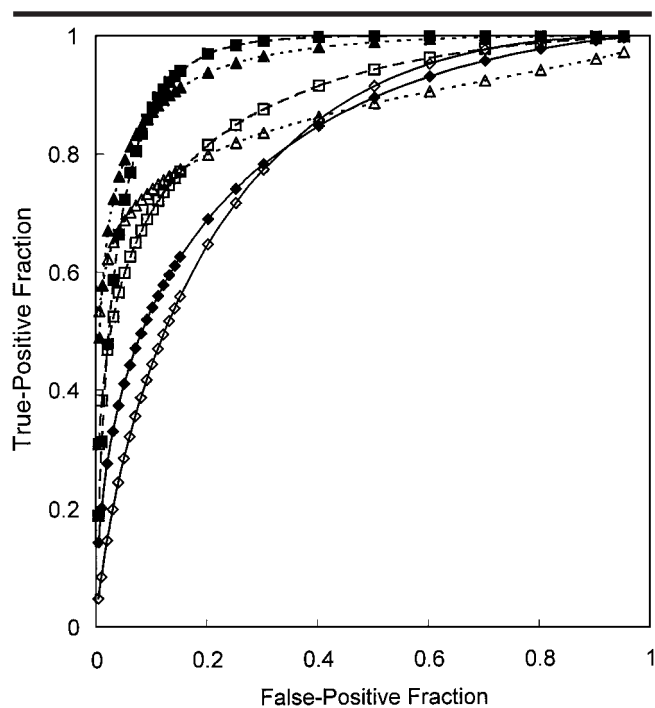


Figure 1. ROC curves show each reader's confidence in differentiating benign from malignant causes of biliary dilatation on the basis of MRCP images alone; on the basis of the combination of MRCP images and T1- and T2-weighted images; and on the basis of the combination of MRCP images, T1- and T2-weighted images, and dynamic images. Diagnostic accuracy with MRCP images and T1- and T2-weighted images was significantly higher than that with MRCP images alone for both readers. \blacklozenge = reader 1, MRCP images alone; \diamond = reader 2, MRCP images alone; \blacksquare = reader 1, MRCP images combined with T1- and T2-weighted images; \square = reader 2, MRCP images combined with T1- and T2-weighted images; \blacktriangle = reader 1, MRCP images combined with T1- and T2-weighted and dynamic images; \triangle = reader 2, MRCP images combined with T1- and T2-weighted and dynamic images.

5, definitely malignant. If the cause of the biliary abnormality was assumed to be malignant, the reasons were chosen from the following findings: visualization of tumor, double duct sign, abrupt obstruction of bile duct, irregularity of obstructed margin, or asymmetric obstruction of the distal margin of the dilated bile duct. Other additional findings were recorded, if present.

At the second step, the readers reviewed less heavily T2-weighted and non-enhanced T1-weighted images simultaneously in addition to the MRCP images; the same five-point scale was used. If the level of confidence was changed at this time, the reason or reasons were recorded.

At the third step, gadolinium-enhanced dynamic images, if available, were added for interpretation, and the cause of abnormality was rated by using the same five-point scale. All three steps of analysis were performed at the same session for each case.

To determine interobserver variability in the assignment of a confidence level to the lesion status, weighted κ values were calculated to measure the degree of agreement between readers. A κ value greater than 0 was considered to indicate positive correlation: marginal, 0.01–0.40; good, 0.41–0.70; and excellent, 0.71–1.00.

Receiver operating characteristic (ROC) curve analysis was performed to compare the results of readings of MRCP images versus the results of readings of the combination of MRCP images and nonenhanced T1-weighted and less heavily T2-weighted images and versus the results of readings of all available images, including gadolinium-enhanced dynamic images. Binormal ROC curves were fitted by using ROCKET 0.9B software (17). The diagnostic capability was determined by calculating the area under the ROC curve (A_z) for each reader. Results were expressed as the mean plus or minus 1 SD. Calculation of the statistical significance of the difference between the areas under the ROC curves for the two readers was performed with use of the univariate z score test by using the same software.

Confidence level ratings of the images were also used to calculate the sensitivity, specificity, and accuracy for each observer in the diagnosis of malignancy with MR images. Ratings of 1 or 2 indicated a reading of a benign lesion; ratings of 4 or 5 indicated a reading of a malignant lesion. Ratings of 3, or possibly malignant, were considered to indicate an incorrect diagnosis. Sensitivity, specificity, and accuracy were calculated as

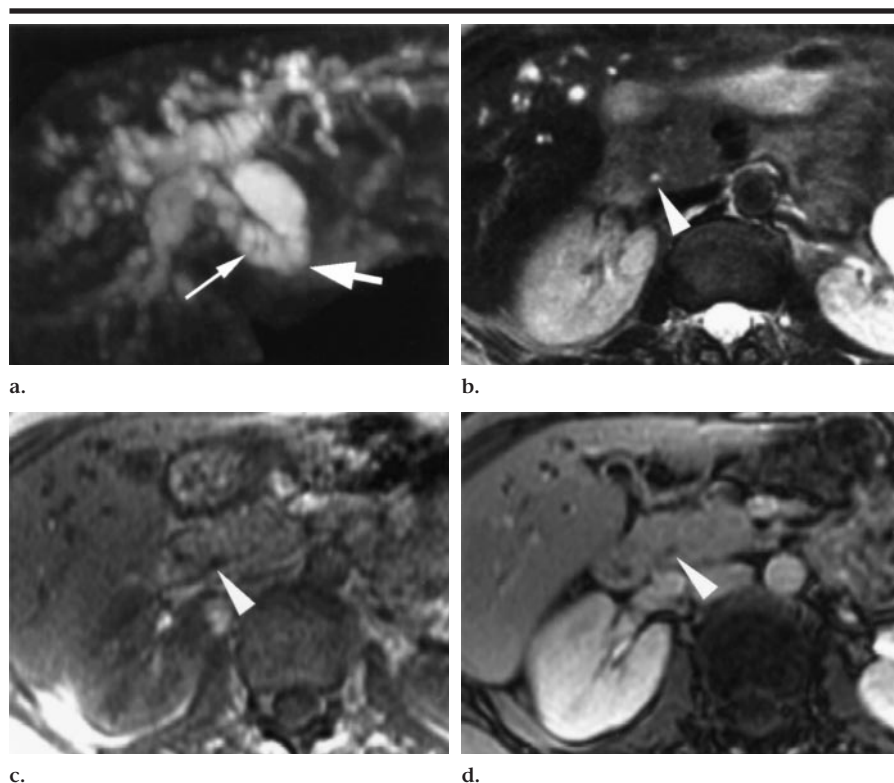


Figure 2. Clinically suspected primary sclerosing cholangitis in a 57-year-old woman with a history of Crohn disease. (a) Coronal maximum intensity projection image reconstructed from heavily T2-weighted MRCP images (fast SE, 12,000/255) shows an abrupt obstruction of the distal common bile duct (thick arrow). A malignant cause was suggested on MRCP images alone for both readers. Extrahepatic insertion of the right posterior hepatic bile duct (thin arrow) into the lower portion of the distal common bile duct is visible. (b) Transverse less heavily T2-weighted image (fast SE, 9,000/144), (c) transverse in-phase GRE image (130/4.2) obtained before the administration of contrast material, and (d) transverse opposed-phase GRE image (130/1.8) obtained after the administration of contrast material show a small, patent distal common duct (arrowhead) and a normal appearance of the surrounding pancreatic parenchyma. Malignancy was excluded correctly with less heavily T2- and T1-weighted images, and the confidence was correctly increased with the postcontrast images for one reader. Ampullary biopsy performed at ERCP showed nonspecific inflammation.

follows: sensitivity = (number of correct diagnoses of malignancy/number of proved malignancies) \times 100, specificity = (number of correct diagnoses of benign cause/number of proved benign causes) \times 100, and accuracy = [(number of correct diagnoses of benign causes + number of correct diagnoses of malignant causes)/number of proved malignant and benign causes] \times 100. The sensitivity, specificity, and accuracy for MRCP images alone were compared with those for the combined images by using the paired Student t test. All P values were two-tailed, and those less than .05 were regarded as showing a statistically significant difference.

RESULTS

The mean diameter of the common bile duct was 13 mm (range, 9–21 mm). In 32

cases, both the bile duct and the pancreatic duct were dilated; in the remaining cases, only the bile duct was dilated.

The κ values for interobserver variability are listed in Table 1. The weighted κ values indicate good to excellent agreement between observers for MR images obtained with all imaging sequences.

Table 2 lists the individual A_z values for interpretation of each image set in terms of the differentiation of benign from malignant causes of biliary dilatation. In this analysis, A_z values for both readers were significantly higher ($P < .05$) for the combination of MRCP images and nonenhanced T1- and less heavily T2-weighted images with or without dynamic images (0.9547 for reader 1, 0.8404 for reader 2) than for MRCP images alone (0.8144 for reader 1, 0.8122 for reader 2). Statistical findings between interpretation of MRCP images alone and interpretation of MRCP

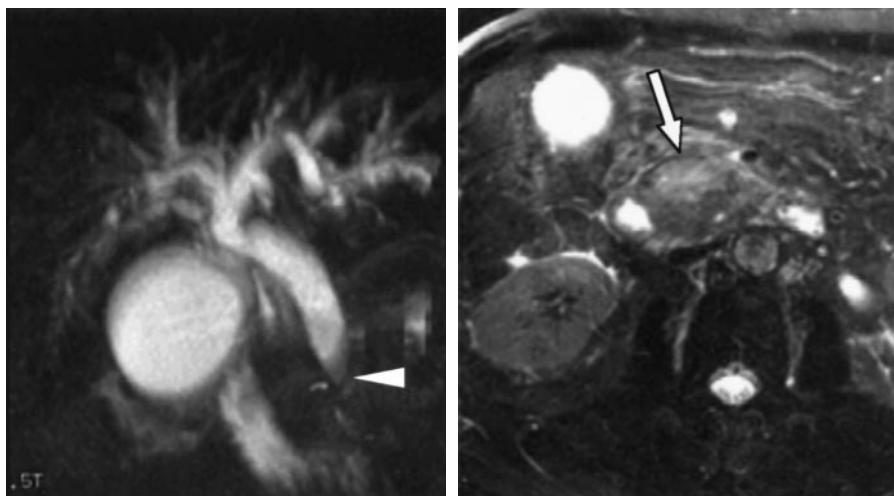


Figure 3. Biliary dilatation in a 70-year-old woman. (a) Coronal maximum intensity projection image reconstructed from MRCP images (fast SE, 14,000/280) shows smooth tapering of the distal common duct (arrowhead) with moderate dilatation of the biliary tree. Differentiation of benign from malignant cause was difficult on MRCP images alone. (b) Transverse less heavily T2-weighted image (fast SE, 10,909/120), (c) transverse precontrast in-phase GRE image (140/4.2), and (d) transverse postcontrast opposed-phase GRE image (120/2.5) clearly show a pancreatic head carcinoma (arrow), which was confirmed at surgery.

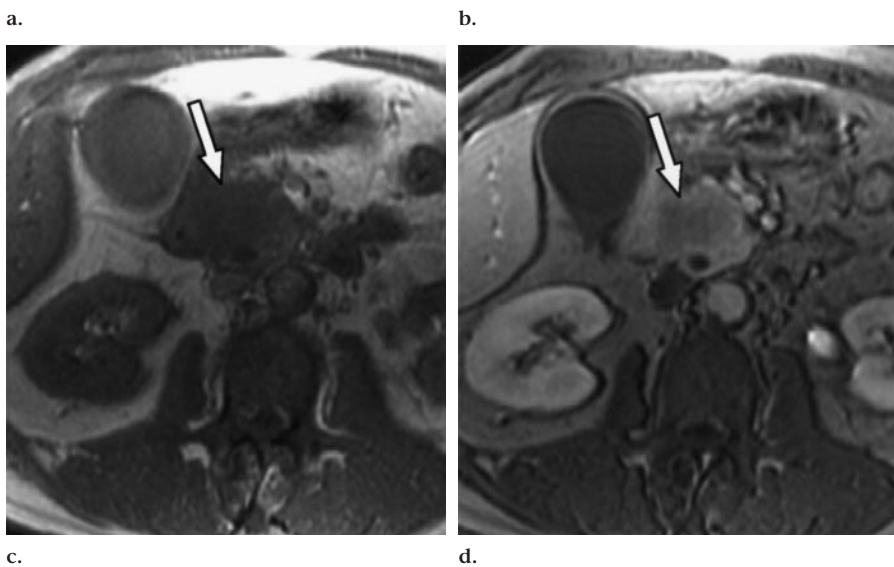


Figure 4. Choledocholithiasis in an 80-year-old woman. (a) Coronal MRCP image (fast SE, 12,100/255) shows an ovoid filling defect (arrowhead) suggestive of a calculus. Another focal bulging shadow (arrow) at the ampullary portion is difficult to characterize on MRCP images alone. (b, c) Transverse less heavily T2-weighted images (fast SE, 6,000/100) show the proximal calculus (arrowhead in b). The focal bulging shadow seen in a has the same appearance as the proximal calculus, and an impacted calculus (arrow in c) in the ampulla is determined confidently.

images with nonenhanced conventional images were significant for both readers (Table 3, Figs 1–4). The difference in A_z values for MRCP images with nonenhanced conventional images and MRCP images with nonenhanced and gadolinium-enhanced dynamic images was not statistically significant (Figs 5, 6). The A_z values for each image set were not statistically different between the readers (Table 4).

Table 5 lists the accuracy, sensitivity, and specificity for the differentiation of benign from malignant causes of biliary abnormalities for each image set for each reader. Overall accuracy, sensitivity, and specificity were statistically significantly higher for MRCP images combined with nonenhanced conventional MR images ($P < .05$) than those for MRCP images alone. Accuracy, sensitivity, and specificity for differentiation of the cause of dilatation by interpreting the combination of MRCP images with nonenhanced and enhanced dynamic MR images were significantly higher than those for MRCP images interpreted alone, but they were not significantly higher than those for MRCP images interpreted with nonenhanced T1- and T2-weighted images. Mean accuracy, sensitivity, and specificity for the two readers increased 19%, 17%, and 20%, respectively (Table 5).

Diagnosis was changed correctly with use of T1- and T2-weighted images in 13 (21%) cases for both readers. When interpretation of dynamic images was added, diagnosis was changed correctly for an additional two (3%) cases for reader 1 and for an additional five (9%) cases for reader 2, as compared with interpretation of MRCP images alone. Diagnosis was changed incorrectly in one case for reader 1 and in two cases for reader 2 when T1- and T2-weighted images were included in addition to MRCP images. When contrast material-enhanced images were added for reader 1, diagnosis was changed incorrectly in two cases as compared with

diagnosis with MRCP images alone and in two cases as compared with diagnosis with MRCP images and T1- and T2-weighted images. For reader 2, diagnosis was not changed incorrectly with inclusion of dynamic MR images as compared with MRCP images alone or MRCP images with T1- and T2-weighted images.

For reader 1, diagnostic confidence correctly increased (ie, the level of confidence increased in true-positive cases and decreased in true-negative cases) in 23 (37%) cases with nonenhanced T1- and T2-weighted images added to MRCP images as compared with MRCP images alone, in 26 (45%) cases with addition of T1- and T2-weighted and gadolinium-enhanced images as compared with MRCP images alone, and in 10 (17%) cases as compared with MRCP images with T1- and T2-weighted images. For reader 2, diagnostic confidence correctly increased in 33 (5%) cases with nonenhanced T1- and T2-weighted images added to MRCP images as compared with MRCP images alone, in 35 (61%) cases with addition of gadolinium-enhanced images as compared with MRCP images alone, and in 14 (24%) cases as compared with MRCP images with T1- and T2-weighted images. The diagnosis was changed correctly in six (29%) of 21 pancreatic carcinomas for reader 1 and four (19%) for reader 2 after T1- and T2-weighted images were added to MRCP images alone. Gadolinium-enhanced images increased the level of confidence by exclusion of tumor in some cases of benign conditions ($n = 7$ for reader 1, $n = 8$ for reader 2) and better visualization of tumor in pancreatic carcinoma ($n = 3$ for reader 1, $n = 4$ for reader 2).

DISCUSSION

Differentiation of benign from malignant biliary obstruction has been one of the challenges in MRCP examinations. The differential diagnosis partly depends on the morphology of the structure, as with direct cholangiography, but relatively lower spatial resolution and lack of injection of contrast material in MRCP sometimes make it difficult to attain a correct diagnosis. In reports in which GRE techniques were used, Wallner et al (8), Ishizaki et al (9), and Hall-Craggs et al (10) reported accuracies of 62%, 30%, and 60%, respectively, in the characterization of biliary obstruction with (8,10) or without (9) the combination of conventional T1- or T2-weighted images. Later, Lee et al (11) attained an improved accuracy of 87% by using a three-dimensional GRE technique.

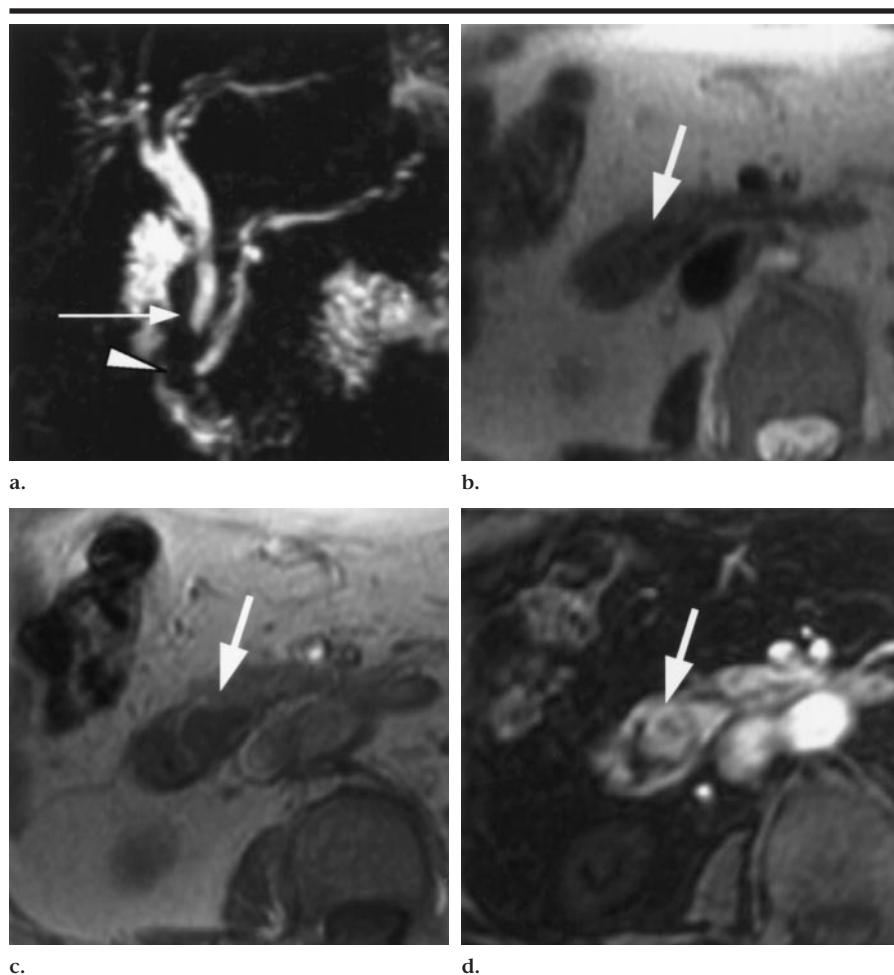


Figure 5. Surgically proved ampullary carcinoma in a 71-year-old woman. (a) Coronal maximum intensity projection image reconstructed from MRCP images (fast SE, 13,200/252) shows mild dilatation of the common bile duct (arrow) and pancreatic duct with short segmental interruption of the ampulla (arrowhead). (b) Transverse less heavily T2-weighted image (fast SE, 10,909/120) and (c) transverse precontrast in-phase GRE image (140/4.2) show soft-tissue signal intensity at the ampullary portion (arrow), but characterization of the lesion is difficult. (d) Transverse postcontrast three-dimensional GRE image (6.9/2.2/31; flip angle, 15°) more clearly demonstrates the focally bulging ampullary mass (arrow), but the differentiation between benignity and malignancy is difficult.

In a study performed by using a two-dimensional fast SE technique in 79 patients, Guibaud et al (2) found further improved accuracy. In their study, MRCP allowed correct determination of a malignant cause of obstruction in 12 of 14 patients, with two additional false-positive cases, which resulted in a sensitivity of 86% and a specificity of 98%. However, Becker et al (13) reported that the distinction between benign and malignant stricture could not be determined in approximately one-third of 43 cases of bile duct stenosis, even though they achieved a sensitivity of 97%–99% and specificity of 95%–97% for detection of bile duct abnormality. Differentiation of pancreatic carcinoma from chronic pancreatitis and be-

nign ampullary stenosis was the main problem.

Although the accuracy of characterization in an initial report (12) in which single-shot half-Fourier acquisition technique was used was not high, Fulcher et al (1) recently reported excellent results in differentiation of causes of bile duct obstruction. In their study of 300 subjects, 32 malignant obstructions were correctly predicted with two false-positive cases, which resulted in a sensitivity of 100% and a specificity of 98%. In that study, they used a half-Fourier rapid acquisition with repeated echoes, or RARE, technique in conjunction with conventional nonenhanced T1-weighted breath-hold spoiled GRE and less heavily T2-weighted breath-

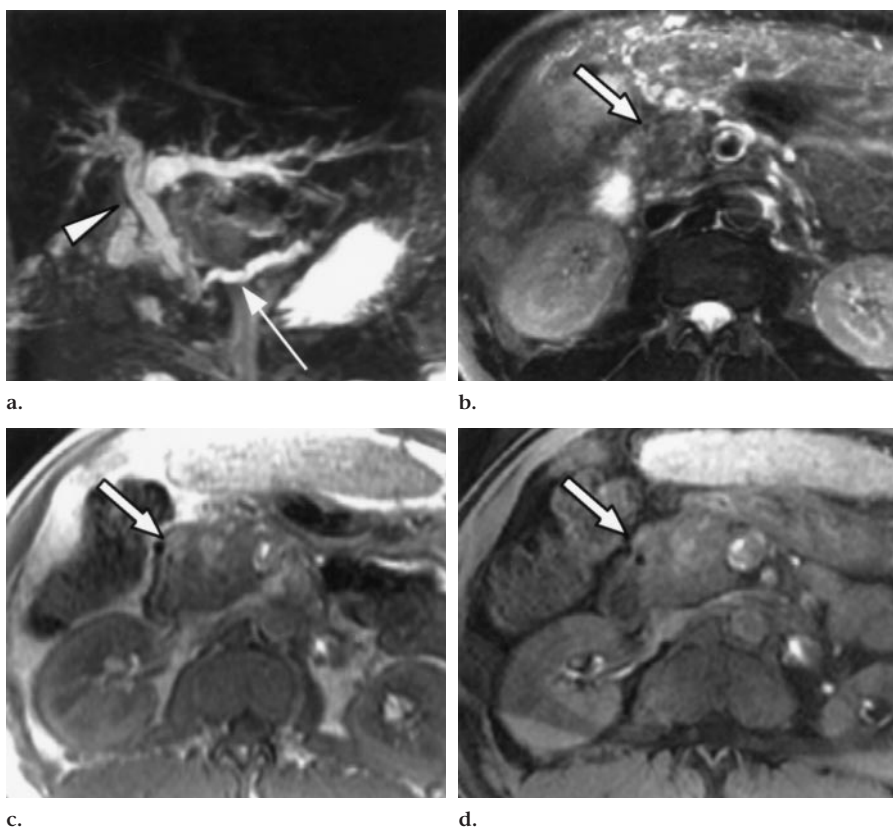


Figure 6. Chronic pancreatitis in a 50-year-old man. (a) Coronal maximum intensity projection image reconstructed from MRCP images (fast SE, 12,000/260) shows dilatation of the biliary tree (arrowhead) and pancreatic duct (arrow). A malignant cause was suggested on the MRCP image. (b) Transverse less heavily T2-weighted image (fast SE, 9,000/120), (c) transverse precontrast in-phase GRE image (120/4.2), and (d) transverse postcontrast fat-saturated GRE image (140/1.8) show focal enlargement and heterogeneous signal intensity of the pancreatic head (arrows). Pancreatic carcinoma was suggested at MR examination; however, pancreaticoduodenectomy revealed chronic pancreatitis and fibrosis but no tumor.

TABLE 4
Statistical Significance of Differences in A_z Values for Reader 1 versus A_z Values for Reader 2

Images	<i>P</i> Value
MRCP only	.7454
MRCP with T1- and T2-weighted	.1160
MRCP, T1- and T2-weighted, and dynamic	.1973

hold fast SE imaging. They did not compare the accuracy between the MRCP images alone and MRCP images with conventional T1- and T2-weighted images. However, we hypothesized that the addition of the T1- and less heavily T2-weighted images might play an important role in improving the diagnostic accuracy over use of MRCP images alone.

Conventional T1- and less heavily T2-weighted images are frequently com-

bined with MRCP images in evaluation of biliary abnormalities (16,18). Those conventional images may improve the specificity of MRCP examinations by allowing visualization of periductal masses and pancreatic parenchymal abnormalities (16). However, the addition of T1- and T2-weighted images and contrast-enhanced images increases the imaging time and cost and decreases patient throughput. Therefore, it is important to determine the specific role of additional conventional T1- and T2-weighted and gadolinium-enhanced images in MRCP examinations.

Our study showed that sensitivity, specificity, and accuracy can be increased 17%–20% when T1- and T2-weighted images are combined with MRCP images for differentiation of benign from malignant causes of biliary dilatation. T1- and T2-weighted images improved diagnostic confidence by allowing more confident exclusion of soft-tissue masses or correct

identification of pancreatic head masses (Figs 2, 3). Benign dilatation can be suggested on MRCP images alone in an appropriate clinical setting, according to the direct cholangiographic examination criteria. However, readers were blinded to the clinical information in this study.

Differential diagnosis between biliary disease and pancreatic tumor often can be achieved by using US or CT. MR imaging and MRCP may be performed in difficult cases. In addition, with the increased use of MRCP in clinical practice, MRCP may be the first diagnostic modality for suspected biliary disease manifesting as painless jaundice. MRCP can provide the correct diagnosis in pancreatic carcinoma with depiction of pancreatic ductal dilatation. MRCP also offers advantages over ERCP by depicting the proximal duct beyond the obstruction. However, pancreatic ductal dilatation can be present in chronic pancreatitis without the presence of tumor. Although the morphologic features of ductal dilatation may be helpful in obtaining a differential diagnosis, direct visualization of the mass is important for correct diagnosis. Fulcher et al (1) also described conventional MR images as helpful in determining tumor extent in most cases.

Polypoid filling defects in the distal common duct are differentiated more confidently with the use of the combination of less heavily T2-weighted images in our study. On MRCP images, biliary calculi are depicted as hypointense filling defects in the high-signal-intensity lumen. Calculi can be differentiated from tumor in most cases, as the calculi may have angulated contours, depending on the location in the bile duct, and are nearly completely surrounded by high-signal-intensity bile. However, sometimes a filling defect from pneumobilia, blood clot, protein plug, or tumor tissue can mimic choledocholithiasis (18,19). When MRCP images alone are used with a long echo time and fat saturation, it may be difficult to differentiate the hypointense calculi with markedly short T2 from soft-tissue lesions with more moderate T2. In this study, one case of impacted stone in the ampulla mimicked a polypoid mass on MRCP images alone; however, it was easily differentiated from a soft-tissue lesion on a less heavily T2-weighted image (Fig 4).

In this study, use of the gadolinium-enhanced dynamic images did not significantly improve the diagnostic accuracy for differentiation of benign from malignant causes of biliary abnormalities. However, the level of confidence increased

TABLE 5
Differentiation of Benign from Malignant Causes of Biliary Dilatation

Parameter	Reader 1			Reader 2		
	MRCP Images Only (n = 62)	MRCP Images with T1- and T2-weighted Images (n = 62)	MRCP Images, T1- and T2-weighted Images, and Dynamic Images (n = 58)	MRCP Images Only (n = 62)	MRCP Images with T1- and T2-weighted Images (n = 62)	MRCP Images, T1- and T2-weighted Images, and Dynamic Images (n = 58)
True-positive*	19	26	23	16	18	19
True-negative*	20	25	24	22	31	31
False-positive*	15	10	8	13	4	1
False-negative*	8	1	3	11	9	7
Accuracy†	63	82	81	61	79	86
Sensitivity†	70	96	88	59	67	73
Specificity†	57	71	75	63	89	97

Note.—Overall accuracy, sensitivity, and specificity are statistically significantly higher for interpretation of MRCP images with T1- and T2-weighted images and for interpretation of MRCP images with T1- and T2-weighted and dynamic images than for interpretation of MRCP images alone for both readers.

* Data are the number of cases.

† Data are percentages.

correctly by 17%–24% as compared with that for MRCP images combined with T1- and T2-weighted images.

The usefulness of dynamic MR imaging in detection and evaluation of local tumor extension or vascular involvement of pancreatic duct adenocarcinomas has been documented by several authors (20–23). Becker et al (13) obtained T1-weighted MR images before and after administration of contrast material in 23 cases in their study of 108 cases. Gadolinium-enhanced T1-weighted images were helpful in differentiation between a soft-tissue mass and an impacted calculus. However, the information provided with the T1-weighted MR images did not alter the diagnosis made with the MRCP images alone. In their study, one plane of the T2-weighted images was obtained without fat saturation; therefore, the soft-tissue anatomy was preserved as on the less heavily T2-weighted images in our study. In most cases in which conventional MR images were helpful in changing or increasing the level of confidence in our study, less heavily T2-weighted MR images were more helpful than T1-weighted images. However, we did not specifically compare T1-weighted images versus less heavily T2-weighted images.

The diagnostic accuracy in this study is modest compared with that in some prior studies with accuracies as high as 98% (1,2). The modesty of diagnostic accuracy in our study may be attributed to several reasons. No clinical information was given to readers during the image analysis. Availability of the medical history, laboratory data, and other cross-sectional imaging data might improve the accuracy (1).

Also, the patient population contained a larger proportion of pancreatic lesions and biliary stenosis noted at the ampullary level.

The reasons for MR examinations in the cases in our study were mainly to further clarify lesions for which the correct diagnosis was difficult to achieve with other imaging examinations. MRCP examinations were part of the comprehensive MR examinations of the upper abdomen, and the patients were not referred specifically for MRCP. Among the 62 cases, 32 (52%) had lesions at the pancreatic or ampullary level, and 24 cases without obstruction also showed biliary dilatation to the level of the ampulla. The difficulty in differentiating benign from malignant biliary dilatation in patients with ampullary lesions has been described in a previous study (13). In the study by Becker et al (13), among the 15 cases for which MRCP was not able to show the cause of biliary dilatation, 14 cases had stenoses at the pancreatic and ampullary levels. In our study, there was still difficulty in a case of chronic pancreatitis with fibrosis mimicking pancreatic carcinoma (Fig 6).

The variability of imaging techniques might affect the relatively lower level of accuracy with use of MRCP images. MRCP images were obtained with two-dimensional fast SE sequences in 34 cases and single-shot fast SE sequences in 28 cases. As the MRCP technique is a rapidly evolving process, the newer and faster single-shot fast SE technique shows better results (1). In about half of the cases in our study, MRCP images were obtained with only a single plane: 28 in the coronal

plane and seven in the transverse plane. Acquisition of both coronal and transverse images also might have improved the accuracy of MRCP images.

Lack of specific diagnosis in most cases of nonspecific biliary dilatation is a limitation of this study. However, as the purpose of this study was to evaluate relative performance with MRCP images alone as compared with that when conventional MR images were included in differentiation of benign from malignant biliary dilatation, clinical and imaging diagnoses with long-term follow-up for benignity in these patients may be sufficient. However, the relatively larger proportion of this group in our study might have some role in decreasing the diagnostic accuracy of using MRCP images alone.

Our results support the recommendation that the MRCP sequence should not replace conventional MR techniques. However, to our knowledge, prior to this study, there have been few data to support this view. We expect that conventional MR sequences are also important in the evaluation of malignant lesions, including pancreatic carcinomas and cholangiocarcinomas, and in the assessment of vascular invasion, lymphadenopathy, and distant metastasis.

In conclusion, our study showed that addition of nonenhanced T1- and less heavily T2-weighted images increased the diagnostic accuracy in differentiation of benign from malignant causes of biliary dilatation. Further addition of gadolinium-enhanced T1-weighted dynamic images did not significantly improve the diagnostic accuracy for differentiating the causes of biliary dilatation but increased

the level of confidence in 17%–24% of cases as compared with that for the combination of MRCP images and T1- and T2-weighted images, especially in cases of biliary dilatation due to pancreatic carcinomas.

References

1. Fulcher AS, Turner MA, Capps GW, Zfass AM, Baker KM. Half-Fourier RARE MR cholangiopancreatography: experience in 300 subjects. *Radiology* 1998; 207:21–32.
2. Guibaud L, Bret PM, Reinhold C, Atri M, Barkun AN. Bile duct obstruction and choledocholithiasis: diagnosis with MR cholangiography. *Radiology* 1995; 197:109–115.
3. Chan YL, Chan ACW, Lam WWM, et al. Choledocholithiasis: comparison of MR cholangiography and endoscopic retrograde cholangiography. *Radiology* 1996; 200:85–89.
4. Barish MA, Yucel EK, Soto JA, et al. MR cholangiography: efficacy of three-dimensional turbo spin-echo technique. *AJR* 1995; 165:295–300.
5. Regan F, Fradin J, Khazan R, Bohlman M, Magnuson T. Choledocholithiasis: evaluation with MR cholangiography. *AJR* 1996; 167:1441–1445.
6. Reinhold C, Taourel P, Bret PM, et al. Choledocholithiasis: evaluation of MR cholangiography for diagnosis. *Radiology* 1998; 209:435–442.
7. Park MS, Yu JS, Kim YH, Kim MJ, Kim JH, Lee S. Acute cholecystitis: comparison of MR cholangiography and US. *Radiology* 1998; 209:781–785.
8. Wallner BK, Schumacher KA, Weidenmaier W, et al. Dilated biliary tract: evaluation with MR cholangiography with a T2-weighted contrast-enhanced fast sequence. *Radiology* 1991; 181:805–808.
9. Ishizaki Y, Wakayama T, Okada Y, et al. Magnetic resonance cholangiography for evaluation of obstructive jaundice. *Am J Gastroenterol* 1993; 88:2072–2077.
10. Hall-Craggs M, Allen CM, Owens CM, et al. MR cholangiography: clinical evaluation in 40 cases. *Radiology* 1993; 189:423–427.
11. Lee MG, Lee HJ, Kim MH, et al. Extrahepatic biliary diseases: 3D MR cholangiopancreatography compared with endoscopic retrograde cholangiopancreatography. *Radiology* 1997; 202:663–669.
12. Regan F, Smith D, Khazan R, et al. MR cholangiography in biliary obstruction using half-Fourier acquisition. *J Comput Assist Tomogr* 1996; 20:627–632.
13. Becker CD, Grossholz M, Becker M, Mentha G, de Peyer R, Terrier F. Choledocholithiasis and bile duct stenosis: diagnostic accuracy of MR cholangiopancreatography. *Radiology* 1997; 205:523–530.
14. Adamek HE, Albert J, Weitz M, et al. A prospective evaluation of magnetic resonance cholangiography in patients with suspected bile duct obstruction. *Gut* 1998; 43:680–683.
15. Holzknacht N, Gauger J, Sackmann M, et al. Breath-hold MR cholangiography with snapshot techniques: prospective comparison with endoscopic retrograde cholangiography. *Radiology* 1998; 206:657–664.
16. Barish MA, Soto JA. MR cholangiopancreatography: techniques and clinical applications. *AJR* 1997; 169:1295–1303.
17. Metz CE. ROCKIT 0.9B [software]. 1998. Available at: <http://www-radiology.uchicago.edu/krl/toppage11.htm>. Accessed January 9, 1999.
18. Ernst O, Calvo M, Sergent G, Mizrahi D, Carpentier F. Breath-hold MR cholangiopancreatography using a HASTE sequence: comparison of single-slice and multislice acquisition techniques. *AJR* 1997; 169:1304–1306.
19. Camus C, Taourel P, Calvet C, Bruel JM. Differentiating stones from tumors of the biliary tree: a new challenge for MR cholangiography? *AJR* 1998; 170:511–512.
20. Reinhold C, Bret PM. Current status of MR cholangiopancreatography. *AJR* 1996; 166:1285–1295.
21. Ichikawa T, Haradome H, Hachiya J, et al. Pancreatic ductal adenocarcinoma: preoperative assessment with helical CT versus dynamic MR imaging. *Radiology* 1997; 202:655–662.
22. Sironi S, De Cobelli F, Zerbi A, et al. Pancreatic adenocarcinoma: assessment of vascular invasion with high-field MR imaging and a phased-array coil. *AJR* 1996; 167:997–1001.
23. Gabata T, Matsui O, Kadoya M, et al. Small pancreatic adenocarcinomas: efficacy of MR imaging with fat suppression and gadolinium enhancement. *Radiology* 1994; 193:683–688.